

- [Browse by subject](#)

- [My account](#)
- [Submit manuscript](#)
- [Register](#)
- [Subscribe](#)

[nature.com](#) [journal home](#) [advance online publication](#) [Article full text](#) [Previous article](#) [Next article](#)

*Nature Photonics* | Article **Highly specific label-free molecular imaging with spectrally tailored excitation-stimulated Raman scattering (STE-SRS) microscopy**

• [Christian W. Freudiger,](#)

• [Wei Min,](#)

• [Gary R. Holtom,](#)

• [Bingwei Xu,](#)

• [Marcos Dantus](#)

•  [& X. Sunney Xie](#)

• [Affiliations](#)

• [Contributions](#)



Science jobs from **naturejobs**

- [Developer](#)
  - Nature Publishing Group
  - London, UK

• [Post a free job](#)

• [More science jobs](#)

**Related content**

• [Corresponding author](#)

*Nature Photonics*(2011)doi:10.1038/nphoton.2010.294

Received 17 August 2010 Accepted 19 November 2010 Published online 16 January 2011

## Abstract

[Abstract](#) [Introduction](#) [Principle](#) [Results](#) [Discussion](#) [Methods](#) [References](#) [Acknowledgements](#)

[Author information](#) [Supplementary information](#)

Label-free microscopy that has chemical contrast and high acquisition speeds up to video rates has recently been made possible using stimulated Raman scattering (SRS) microscopy. SRS imaging offers high sensitivity, but the spectral specificity of the original narrowband implementation is limited, making it difficult to distinguish chemical species with overlapping Raman bands. Here, we present a highly specific imaging method that allows mapping of a particular chemical species in the presence of interfering species, based on tailored multiplex excitation of its vibrational spectrum. This is implemented by spectral modulation of a broadband pump beam at a high frequency (>1 MHz), allowing detection of the SRS signal of the narrowband Stokes beam with high sensitivity. Using the scheme, we demonstrate quantification of cholesterol in the presence of lipids, and real-time three-dimensional spectral imaging of protein, stearic acid and oleic acid in live *Caenorhabditis elegans*.

## Figures at a glance

[left](#)

1. Figure 1: Principle of SRS.

- [Email](#)
- [Download PDF](#)
- [Download citation](#)
- [Order reprints](#)
- [Rights and permissions](#)
- [Share/bookmark](#)

◦ [Connotea](#)

◦ [CiteULike](#)

◦ [Facebook](#)

◦ [Twitter](#)

◦ [Delicious](#)

◦ [Digg](#)

## Articles

1. [Nonlinear silicon photonics](#)

*Nature Photonics* 30 Jul 2010

2. [Coherent coupling between distant excitons revealed by two-dimensional nonlinear hyperspectral imaging](#)

*Nature Photonics* 19 Dec 2010

3. [Raman injection laser](#)

*Nature* 24 Feb 2005

4. [Ultralong quantum optical data storage using an optical locking technique](#)

*Nature Photonics* 23 Aug 2009

5. [Dicke quantum phase transition with a superfluid gas in an optical cavity](#)

*Nature* 29 Apr 2010

[View all](#)

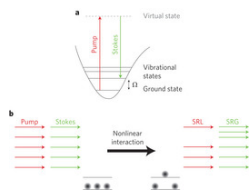
## Open innovation challenges

• [Low-Volume Liquid Dispersion Mechanism](#)



Deadline: Feb 20 2011 Reward: \$25,000 USD

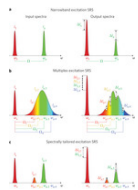
The Seeker is looking for mechanisms to enable dispersion of a fluid sample of 40 nanoliters (nl) ov...



a, Energy diagram of SRS. If the difference frequency of pump and Stokes beams is resonant with a molecular vibration, SRS occurs and a molecule of the sample is excited from its ground state to the vibrational excited state. b, As a result, a pump photon of the excitation field is annihilated (SRL, stimulated Raman loss) and a Stokes photon is created (SRG, stimulated Raman gain) as required from energy conservation.

[See larger](#)

## 2. Figure 2: Excitation schemes of SRS.



a, Narrowband excitation. Narrowband laser beams at pump frequency  $\omega_p$  and Stokes frequency  $\omega_s$  excite a single molecular vibration  $\Omega$ . The resulting SRL or SRG of the pump or Stokes intensity is measured. b, Multiplex excitation. The pump beam is broadband to excite multiple molecular vibrations  $\Omega_i$  of the sample simultaneously. A spectral component  $I_{p,i}$  with frequency  $\omega_{p,i}$  experiences an intensity loss  $\Delta I_{p,i}$  when its frequency difference with the narrowband Stokes beam  $\Delta\omega_i = \omega_{p,i} - \omega_s$  matches  $\Omega_i$ . The total intensity gain of the Stokes beam  $\Delta I_s = \sum_i \Delta I_{s,i}$  originates from the total SRS of all molecular vibrations of the sample. Micro-spectroscopy is performed by dispersing the transmitted pump light onto a multi-element detector and measuring the individual  $\Delta I_{p,i}$ . c, Spectrally tailored excitation. The broadband pump spectrum is shaped to selectively excite only vibrations of a target molecule (for example,  $\Omega_1$  and  $\Omega_3$ ) and avoid frequencies resonant with interfering species (such as  $\Omega_2$  and  $\Omega_4$ ). The total  $\Delta I_s$ , which only contains contributions  $\Delta I_{s,1}$  and

Powered by: **INNOCENTIVE**

[More challenges](#)

## Top content

## Emailed

### 1. [Sequential femtosecond X-ray imaging](#)

*Nature Photonics* 09 Jan 2011

[View all](#)

## Downloaded

### 1. [Sequential femtosecond X-ray imaging](#)

*Nature Photonics* 09 Jan 2011

### 2. [Scale-free optics and diffractionless waves in nanodisordered ferroelectrics](#)

*Nature Photonics* 19 Dec 2010

### 3. [Single-molecule imaging by optical absorption](#)

*Nature Photonics* 09 Jan 2011

### 4. [Stable optical lift](#)

*Nature Photonics* 05 Dec 2010

### 5. [Time-reversed ultrasonically encoded optical focusing into scattering media](#)

*Nature Photonics* 16 Jan 2011

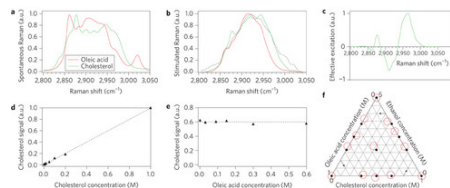


reflection-type pulse-shaper by dispersing the broadband beam with a grating onto an SLM. In- and out-going beams (arrows) are separated by a small spatial separation on a splitting mirror (M). Successive polarization modulation (Pockels cell) and passing through a polarization analyser creates a spectrally modulated pump beam, which switches between originally *s*- and *p*-polarized spectral components. Pump and Stokes beams are spatially overlapped with a dichroic mirror (DM), temporally synchronized with electronics, and aligned into a laser-scanning microscope with scanning mirrors, an objective lens (OL) and a condenser (C). After passing through the sample (S), the pump beam is blocked with a filter (F), and the Stokes beam is detected with a large-area InGaAs photodiode (PD). The signal is analysed with a lock-in amplifier locked into the modulation of the Pockels cell to provide the intensity of a pixel.



[See larger](#)

## 5. Figure 5: Characterization of STE-SRS.

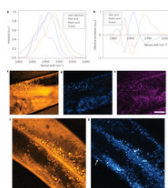


a, Spontaneous Raman spectra of cholesterol (green) and oleic acid (red), which have no isolated Raman vibrations but distinct Raman signatures. b, Expected SRS spectra for cholesterol (green) and oleic acid (red) calculated by normalizing the spontaneous Raman spectra with the laser excitation spectrum (black dotted). c, Excitation mask for selective detection of cholesterol (target species) in the presence of oleic acid (interfering species) generated from the SRS spectra shown in b, satisfying equations (3) using the procedure described in the text. d, Linear dependence of the STE-SRS signal on concentrations of cholesterol allows for straightforward signal quantification. e, STE-SRS allows interference-free detection. STE-SRS signal with the excitation mask shown in c as a function of oleic acid concentration at constant cholesterol concentration (0.6 M) dissolved in

deuterated chloroform, showing no false signal increase due to the increasing concentration of interferent. f, STE-SRS allows suppression against interfering species in a three-component system. Ternary plot of mixtures of cholesterol, oleic acid and ethanol solutions in deuterated chloroform. Solid dots show actual concentration of the mixtures and red circles show measurement with STE-SRS.

[See larger](#)

## 6. Figure 6: Imaging of lipid storage in *C. elegans*.



a, SRS spectra of oleic acid (cyan), stearic acid (magenta) and protein (orange) as computed from the spontaneous Raman library by normalizing with the measured laser excitation spectrum (dotted line). b, Spectral masks computed from spectra in a and used for the imaging. c–e, Spectral images taken from the same area of a *C. elegans*, applying spectral masks for protein (c), oleic acid (d) and stearic acid (e). Comparison of d and e shows that oleic and stearic acid deposits co-localize and that there are no isolated deposits of either species. Comparison of c and d shows that the lipid deposits further co-localize with protein-dense organelles. f,g, Spectral images with protein and oleic acid masks, respectively, from a different region in the worm, further investigate this aspect. Arrows highlight both subdermal and intestinal lipid storage depots. Imaging speed: 30 s per frame, with 512 × 512 sampling. Scale bars, 25 μm.

[See larger](#)

right

## Introduction

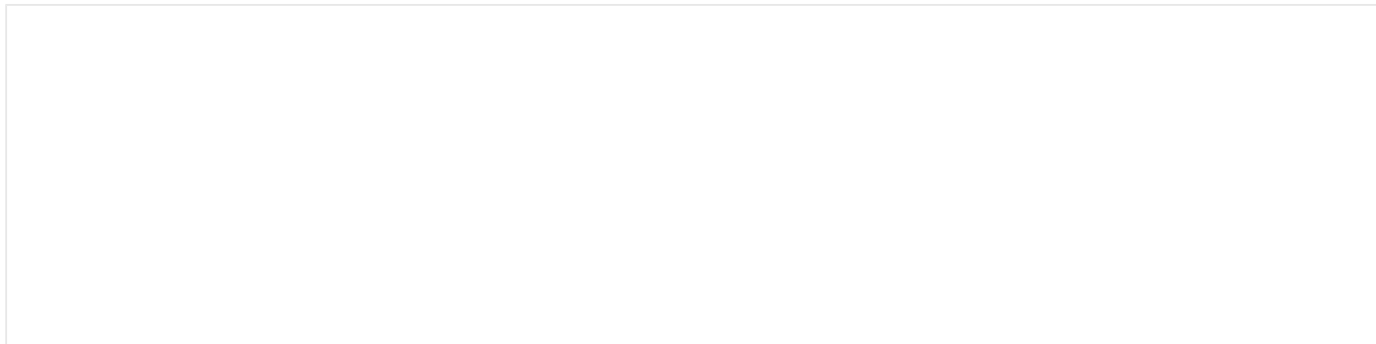
[Abstract](#)[Introduction](#)[Principle](#)[Results](#)[Discussion](#)[Methods](#)[References](#)[Acknowledgements](#)

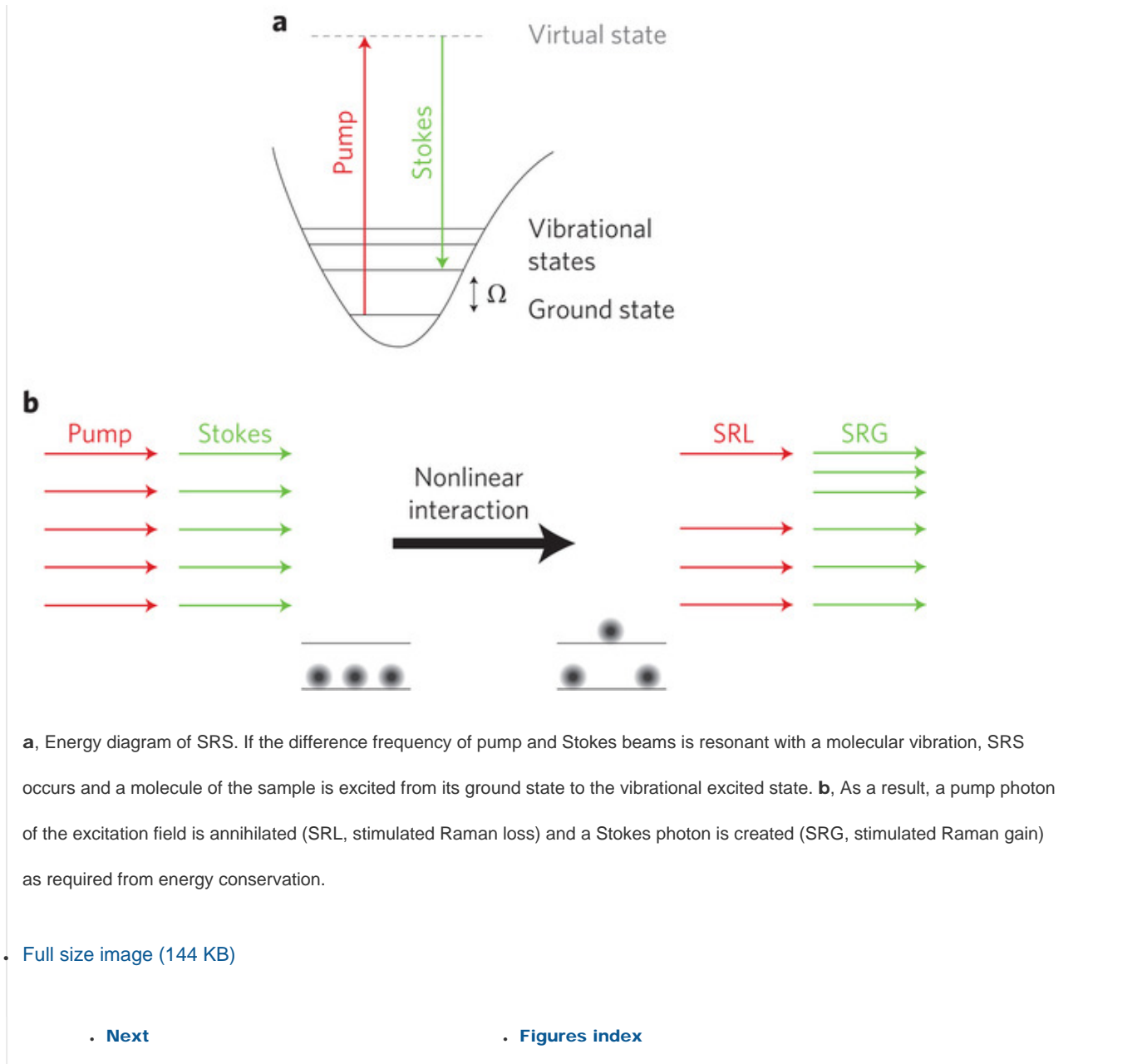
[Author information](#)[Supplementary information](#)

Recently, there has been an increase in the level of interest in label-free biomedical imaging based on vibrational spectroscopy. It is particularly advantageous in the imaging of small molecules such as metabolites and drugs, because the use of fluorophores often introduces perturbations and is subject to photobleaching. Recent advances in coherent Raman scattering (CRS) microscopy, including coherent anti-Stokes Raman scattering (CARS)<sup>1, 2, 3</sup> and stimulated Raman scattering (SRS) microscopy<sup>4, 5, 6, 7</sup>, have led to orders of magnitude higher sensitivity than conventional Raman microscopy, and imaging speeds up to video rates for *in vivo* imaging<sup>8, 9</sup>.

In CRS, the sample is coherently excited by two lasers, one at the pump frequency  $\omega_p$  and the other at the Stokes frequency  $\omega_s$ . When their frequency difference  $\Delta\omega = \omega_p - \omega_s$  matches an intrinsic molecular vibration of the sample of frequency  $\Omega$ , both CARS and SRS occur due to the nonlinear interaction of molecules with the laser pulses (Fig. 1a). In CARS, a signal is generated at the new anti-Stokes frequency  $\omega_{aS} = 2\omega_p - \omega_s$ . In SRS, a pump photon is converted to a Stokes photon when a molecule is excited from the vibrational ground state into the first vibrational excited state. SRS therefore results in an intensity loss  $\Delta I_p$  of the pump beam intensity  $I_p$ , and an intensity gain  $\Delta I_s$  of the Stokes beam intensity  $I_s$  (Fig. 1b).

Figure 1: Principle of SRS.





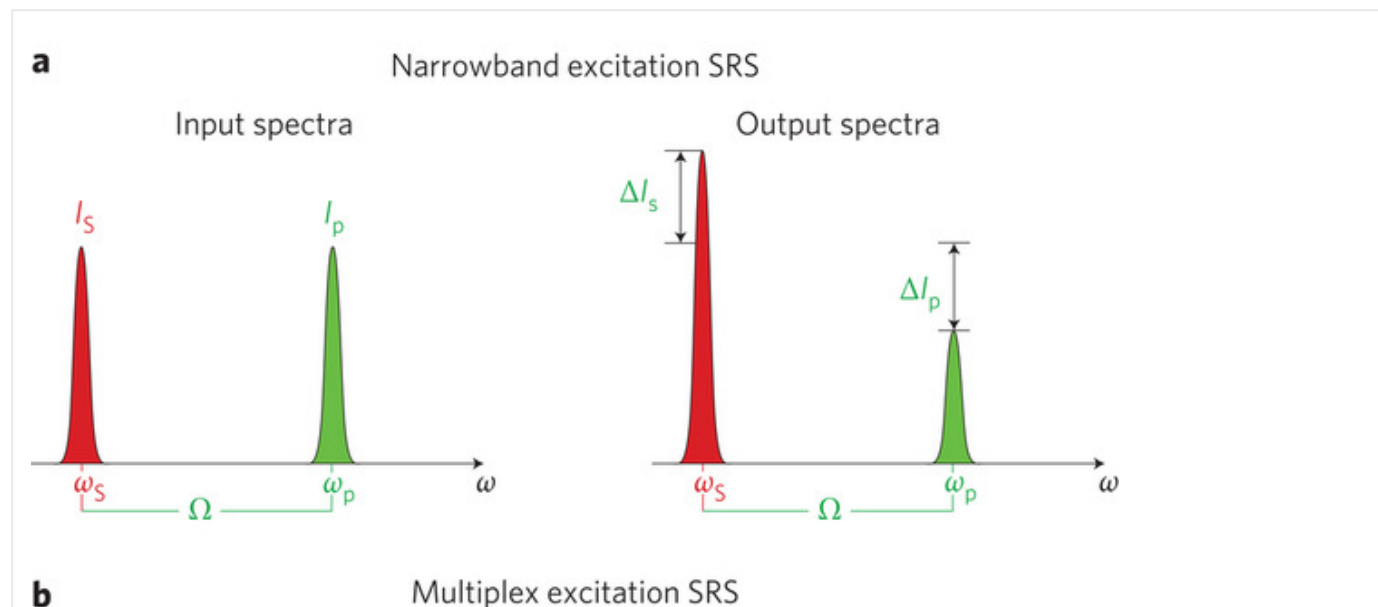
figure

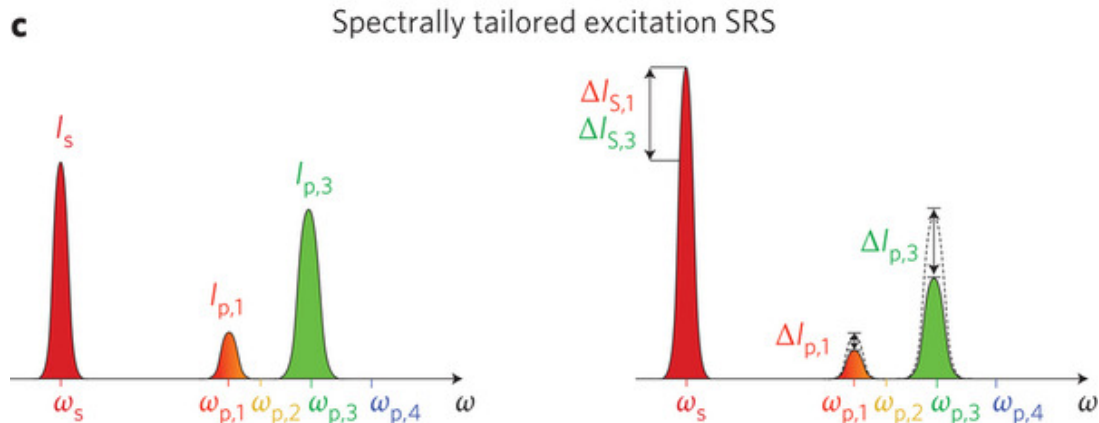
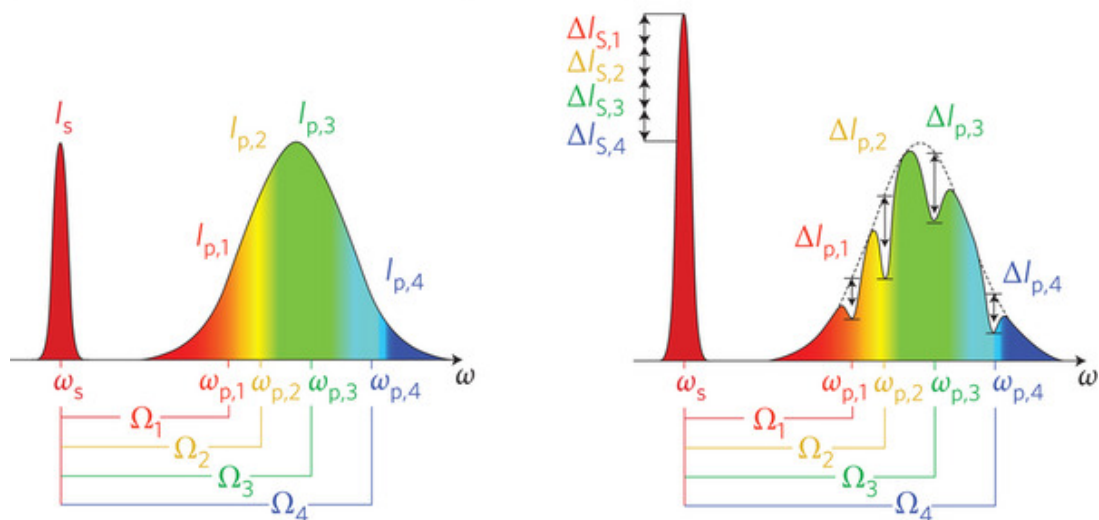
CARS suffers from a non-resonant background signal, which is present even without vibrational resonance<sup>10</sup>. SRS is free from this complication, and the SRS spectra are identical to those of spontaneous Raman scattering, allowing easy assignment based on Raman literature. Furthermore, its sensitivity is approaching the shot-noise limit, and its signal

SRS microscopy under biocompatible excitation conditions was recently demonstrated through the implementation of a high-frequency modulation scheme to detect the relatively low SRS signal in the presence of laser noise. This also allows separation of the SRS signal from slow variations of the transmitted laser intensity due to linear scattering and absorption by the sample during raster scanning of the overlapped foci of the pump and Stokes beams<sup>5, 6, 7</sup>. To do so, either the pump or the Stokes beam is modulated at a high frequency and the modulation transfer to the other beam due to SRS of the sample is detected with phase-sensitive detection. As laser noise typically occurs at low frequencies, we use a high modulation frequency (>1 MHz) to achieve a near shot-noise-limited sensitivity of  $(\Delta I/I) < 10^{-8}$  for an averaging time of 1 s, allowing superb sensitivity in biological samples at moderate laser power<sup>5</sup>.

In the original implementation of SRS microscopy, we used narrowband laser beams (transform-limited picosecond pulse widths) to excite a single Raman-active vibrational mode (Fig. 2a)<sup>5, 9</sup>. However, other vibrational modes of the same species were not excited. This approach therefore does not take full advantage of the chemical specificity of Raman scattering and fails to specifically detect molecules with overlapping Raman bands.

Figure 2: Excitation schemes of SRS.





a, Narrowband excitation. Narrowband laser beams at pump frequency  $\omega_p$  and Stokes frequency  $\omega_s$  excite a single molecular vibration  $\Omega$ . The resulting SRL or SRG of the pump or Stokes intensity is measured. b, Multiplex excitation. The pump beam is broadband to excite multiple molecular vibrations  $\Omega_i$  of the sample simultaneously. A spectral component  $I_{p,i}$  with frequency  $\omega_{p,i}$  experiences an intensity loss  $\Delta I_{p,i}$  when its frequency difference with the narrowband Stokes beam  $\Delta\omega_i = \omega_{p,i} - \omega_s$  matches  $\Omega_i$ . The total intensity gain of the Stokes beam  $\Delta I_s = \sum_i \Delta I_{s,i}$  originates from the total SRS of all molecular vibrations of the sample.

Micro-spectroscopy is performed by dispersing the transmitted pump light onto a multi-element detector and measuring the individual  $\Delta I_{p,i}$ . c, Spectrally tailored excitation. The broadband pump spectrum is shaped to selectively excite only vibrations of a target molecule (for example,  $\Omega_1$  and  $\Omega_3$ ) and avoid frequencies resonant with interfering species (such as  $\Omega_2$  and  $\Omega_4$ ). The total  $\Delta I_s$ , which only contains contributions  $\Delta I_{s,1}$  and  $\Delta I_{s,3}$  of the target molecule, is measured with a single-element detector.

- [Full size image \(347 KB\)](#)

- [Previous](#)

- [Next](#)
- [Figures index](#)

[figure](#) [figure](#)

Instead of using two narrowband pulses, we use a pump beam with a broad bandwidth and a Stokes beam with a narrow bandwidth, so that a wide spectral range of vibrational frequencies can be excited simultaneously<sup>11</sup>. Such multiplex excitation (Fig. 2b) has previously been performed in micro-spectroscopy by using an array detector and slow sample scanning<sup>4, 12, 13, 14</sup>. However, such micro-spectroscopy is not compatible with high-sensitivity detection, because the high-frequency modulation described above cannot be used easily. Here, we present spectrally tailored excitation SRS (STE-SRS) microscopy, which provides images of a particular chemical species through the collective excitation of selected vibrational frequencies (Fig. 2c). Such targeted excitation provides chemical selectivity based on full Raman signatures, and allows fast quantification and mapping of the targeted species even in the presence of interfering species.

## Principle

[Abstract](#)[Introduction](#)[Principle](#)[Results](#)[Discussion](#)[Methods](#)[References](#)[Acknowledgements](#)

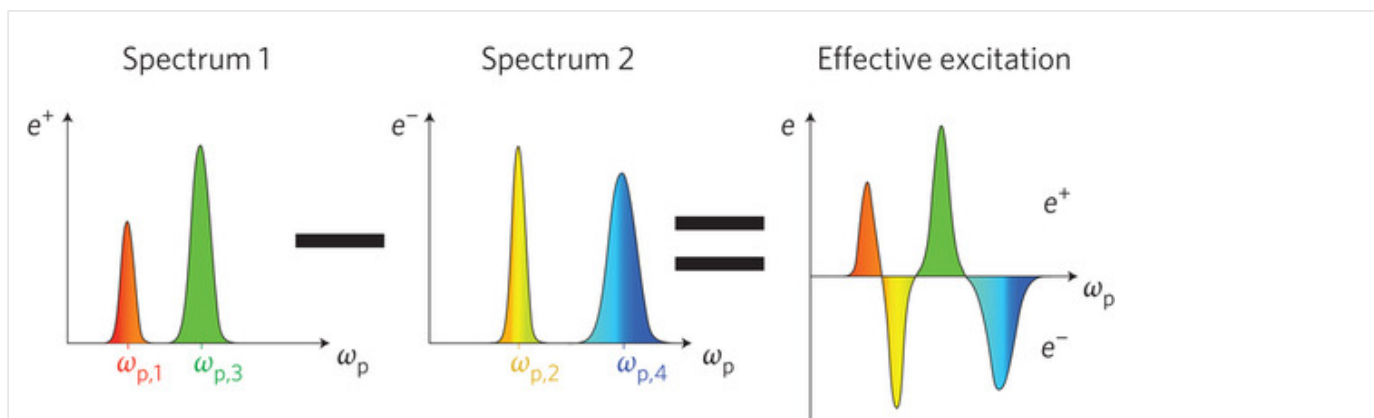
[Author information](#)[Supplementary information](#)

In STE-SRS we use multiplex excitation with a broadband pump and a narrowband Stokes beam. The general principle is that one can tailor the pump spectrum so that it predominantly probes the vibrational resonances of a target species (for example,  $\Omega_1$  and  $\Omega_3$  in Fig. 2c). This is done by masking the spectral components of the broadband pump pulse using a pulse-shaper with a spatial light modulator (SLM)<sup>15</sup>. We then detect the total intensity of the narrowband Stokes beam with a single photodiode, instead of multiplexed spectral detection as in micro-spectroscopy<sup>4</sup>.

However, this first excitation spectrum  $e^+(\omega_p)$  also excites residual signal from interfering species. To discriminate against such interference, we use another excitation spectrum  $e^-(\omega_p)$ , which mainly probes the vibrational resonances of

the interfering species (for example,  $\Omega_2$  and  $\Omega_4$  in Fig. 3), then measure the SRS difference signal between the two excitation spectra, thereby causing the residual signal from interfering species to vanish.

Figure 3: Spectral modulation scheme.



Spectrally tailored excitation allows the targeting of a vibrational resonance that is excited, but it does not directly improve chemical specificity over narrowband excitation because there is no mechanism to suppress signal from overlapping bands of interfering species. In STE-SRS, the broadband pump spectrum is therefore shaped twice. The first spectrum  $e^+(\omega_p)$  mainly contains spectral components resonant with the target species ( $\Omega_1$  and  $\Omega_3$ ). The second spectrum  $e^-(\omega_p)$  mainly contains spectral components resonant with the interfering species ( $\Omega_2$  and  $\Omega_4$ ) and is weighted to cancel out the interfering signal generated by  $e^+(\omega_p)$ . The difference SRS signal from  $e^+(\omega_p)$  and  $e^-(\omega_p)$  can therefore be freed from all interfering contributions. For simplicity, the two spectra can be combined into one effective excitation mask  $e(\omega_p) = e^+(\omega_p) - e^-(\omega_p)$ . Such subtraction can be implemented for real-time imaging by modulating between the two excitation spectra at high frequency and extracting the resulting modulation transfer with a lock-in amplifier.

• [Full size image \(95 KB\)](#)

• [Previous](#)

• [Next](#)

• [Figures index](#)

figure figure

In a mixture of  $n$  chemical species, the contribution of a particular chemical species  $i$  to the detected SRS difference signal is linearly dependent on its concentration  $c_i$ , its Raman spectrum  $\sigma_i(\Omega = \omega_p - \omega_S)$  and the spectrally shaped

broadband pump beam, alternating between two excitation spectra  $e^+(\omega_p)$  and  $e^-(\omega_p)$ :

$$c_i \cdot \left[ \int \sigma_i(\omega_p - \omega_s) \cdot e^+(\omega_p) d\omega_p - \int \sigma_i(\omega_p - \omega_s) \cdot e^-(\omega_p) d\omega_p \right] \\ = c_i \cdot \int \sigma_i(\omega_p - \omega_s) \cdot e(\omega_p) d\omega_p \quad (1)$$

For simplicity, the alternating spectra can be denoted as an excitation mask  $e(\omega_p) = e^+(\omega_p) - e^-(\omega_p)$ , as illustrated in Fig. 3, in which positive contributions represent  $e^+(\omega_p)$  and negative contributions  $e^-(\omega_p)$ .

We can now choose a particular excitation mask  $e_j(\omega_p)$  to selectively probe a target species  $j$  in the presence of the other species. We do so by fulfilling

$$\int \sigma_i(\omega_p - \omega_s) \cdot e_j(\omega_p) d\omega_p = 0 \quad \text{for } i \neq j \\ \int \sigma_i(\omega_p - \omega_s) \cdot e_j(\omega_p) d\omega_p \neq 0 \quad \text{for } i = j \quad (2)$$

In other words, the excitation mask  $e_j(\omega_p)$  for species  $j$  is orthogonal to every interfering species. Hence, the contribution of each interfering species to the SRS signal vanishes, independent of its concentration, and the measured signal only reflects the abundance of the target species  $j$ .

In practice, the broadband pump beam can only be shaped as a collection of  $N$  discrete spectral components, and the integral in equation (2) becomes a summation over all spectral components  $k$

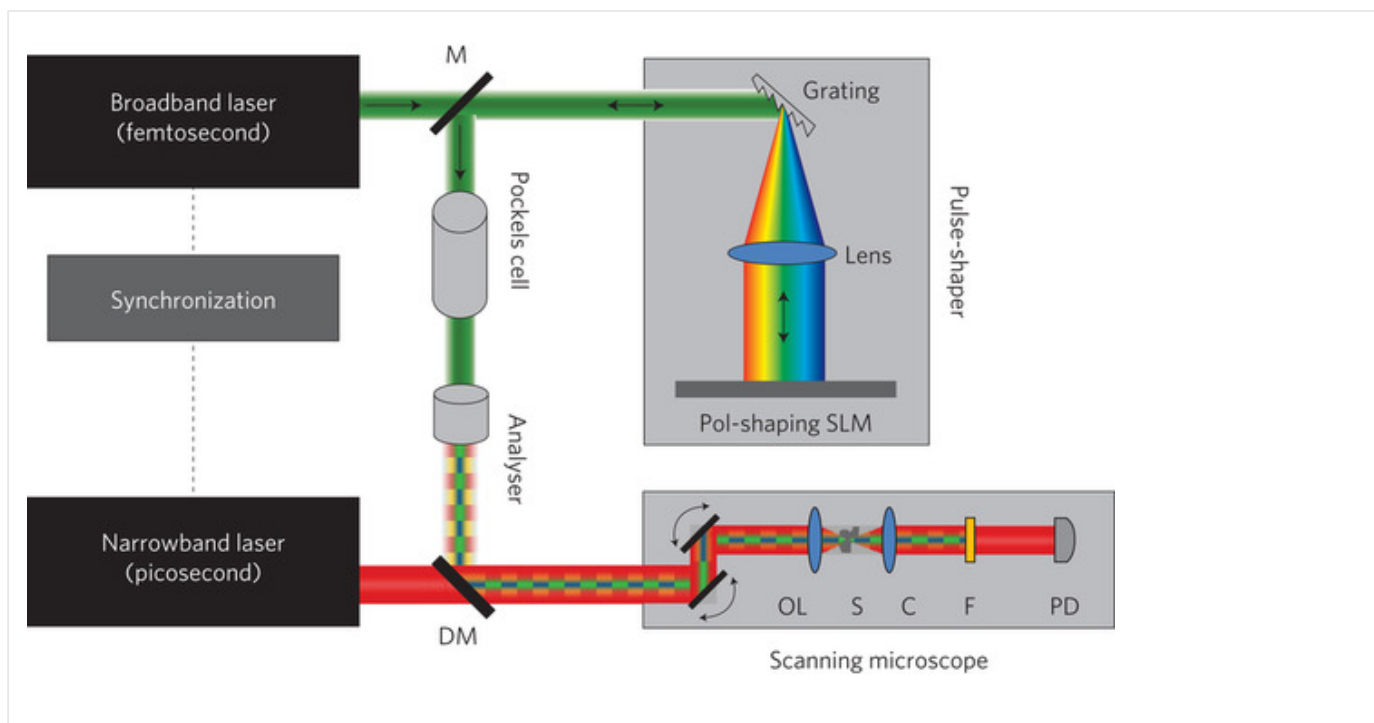
$$\sum_k^N \sigma_i^k \cdot e_j^k = 0 \quad \text{for } i \neq j \\ \sum_k^N \sigma_i^k \cdot e_j^k \neq 0 \quad \text{for } i = j \quad (3)$$

If the total number of species in the sample  $n$  is equal to the number of spectral components  $N$ ,  $e_j^k$  is uniquely determined by equation (3) and can be calculated by the inverse matrix of  $\sigma_i^k$ . The only inputs required are the spontaneous

Raman spectra of all the species involved. Normally the total number of interfering species in a sample is much less than  $N$  (typically 80 in our implementation), and equation system (3) is underdetermined. We therefore calculate the Moore–Penrose pseudo-inverse of  $\sigma^k$ . This procedure is similar to the chemometric method known as classical least squares (CLS), that is, projecting the target spectrum onto the subspace orthogonal to all interfering spectra<sup>16</sup>.

To detect the difference SRS signal in real time and with high sensitivity, we modulate between the two excitation spectra at high frequency (4 MHz). To do so, we combine a polarization pulse-shaper with an SLM, a polarization modulator and a polarization analyser (Fig. 4). Spectral components of the first excitation spectrum are  $s$ -polarized, and components of the second excitation spectrum are  $p$ -polarized. Fast switching between the two excitation masks is achieved by the Pockels cell. After passing through the polarization analyser, the broadband pump beam is again linearly polarized and spectrally modulated. Different target species  $j$  can then be selected by loading different polarization masks onto the SLM between consecutive image frames.

Figure 4: STE-SRS microscopy setup.



Individual spectral components of the broadband pump beam are polarization-shaped in a reflection-type pulse-shaper by dispersing the broadband beam with a grating onto an SLM. In- and out-going beams (arrows) are separated by a small spatial separation on a splitting mirror (M). Successive polarization modulation (Pockels cell) and passing through a polarization analyser creates a spectrally modulated pump beam, which switches between originally *s*- and *p*-polarized spectral components. Pump and Stokes beams are spatially overlapped with a dichroic mirror (DM), temporally synchronized with electronics, and aligned into a laser-scanning microscope with scanning mirrors, an objective lens (OL) and a condenser (C). After passing through the sample (S), the pump beam is blocked with a filter (F), and the Stokes beam is detected with a large-area InGaAs photodiode (PD). The signal is analysed with a lock-in amplifier locked into the modulation of the Pockels cell to provide the intensity of a pixel.

• [Full size image \(164 KB\)](#)

• [Previous](#)

• [Next](#)

• [Figures index](#)

[figure](#) [figure](#)

If such spectral modulation is performed at a high frequency (higher than the low-frequency laser noise), no further amplitude modulation is required for the high-sensitivity detection of SRS. We measure the modulation transfer to the Stokes beam with a phase sensitivity detector (lock-in amplifier) identical to the implementation of narrowband SRS microscopy<sup>5</sup>. The amplitude of the transferred modulation is described by equation (1), as the phase-sensitive detector interprets the in and out phase signals as the first and second excitation spectra, respectively, and automatically gives the difference signal. STE-SRS has the advantage that it combines the high sensitivity of high-frequency modulation with improved spectral specificity of multiplex excitation. STE-SRS is also readily compatible with beam-scanning microscopy and allows for fast imaging speeds and real-time image display.

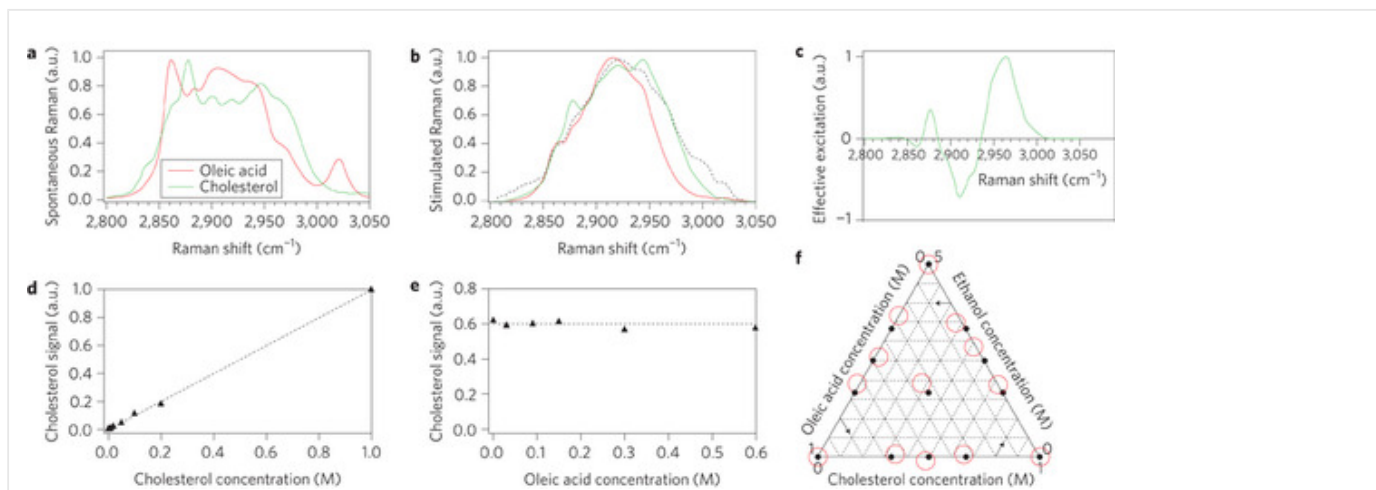
## Results

[Abstract](#)[Introduction](#)[Principle](#)[Results](#)[Discussion](#)[Methods](#)[References](#)[Acknowledgements](#)

[Author information](#)[Supplementary information](#)

We first characterized the STE-SRS signal in a two-component solution of cholesterol and oleic acid, which have overlapping Raman bands. Figure 5a shows the spontaneous Raman spectra of the two compounds, and Fig. 5b the SRS spectra for a particular broadband pump spectrum (dotted line). We calculated the excitation mask for the detection of cholesterol (target species) in the presence of oleic acid (interfering species) from the SRS spectra (Fig. 5c) according to equations (3).

Figure 5: Characterization of STE-SRS.



a, Spontaneous Raman spectra of cholesterol (green) and oleic acid (red), which have no isolated Raman vibrations but distinct Raman signatures. b, Expected SRS spectra for cholesterol (green) and oleic acid (red) calculated by normalizing the spontaneous Raman spectra with the laser excitation spectrum (black dotted). c, Excitation mask for selective detection of cholesterol (target species) in the presence of oleic acid (interfering species) generated from the SRS spectra shown in b, satisfying equations (3) using the procedure described in the text. d, Linear dependence of the STE-SRS signal on concentrations of cholesterol allows for straightforward signal quantification. e, STE-SRS allows interference-free detection. STE-SRS signal with the excitation mask shown in c as a function of oleic acid concentration at constant cholesterol concentration (0.6 M) dissolved in deuterated chloroform, showing no false signal increase due to the increasing concentration of interferent. f, STE-SRS allows suppression against interfering species in a three-component system. Ternary plot of mixtures of cholesterol, oleic acid and ethanol solutions in deuterated chloroform. Solid dots show actual concentration of the mixtures and red circles

show measurement with STE-SRS.

• [Full size image \(182 KB\)](#)

• [Previous](#)

• [Figures index](#)

[figure](#) [figure](#)

For this excitation mask the SRS difference signal is indeed linear with concentration of cholesterol ([Fig. 5d](#)) and independent of the concentration of oleic acid ([Fig. 5e](#)). STE-SRS can suppress against signals from interfering species that are up to ~2,000× stronger ([Supplementary Fig. S1b](#)), because laser intensity fluctuations of individual spectral components of a mode-locked laser are common-mode noise and can be cancelled out. Such strong discrimination against interfering species is not possible with sequential measurements of different Raman bands by narrowband excitation because the signal fluctuations of different bands are uncorrelated. The detection limit of STE-SRS for cholesterol is 5 mM with 1 s time constant ([Supplementary Fig. S1a](#)).

We further demonstrated that STE-SRS can distinguish more than two species. We prepared 13 different three-component solutions with varying concentrations of cholesterol, oleic acid and ethanol in deuterated chloroform. For each of the solutions we sequentially applied three excitation masks ([Supplementary Fig. S2c](#)), which were calculated for the selective detection of each of the three compounds in the presence of the other two, based on the spontaneous Raman spectra show in [Supplementary Fig. S2a](#). We used the signal from the pure solutions to calibrate the instrument and made use of the linear concentration dependence of spectral SRS imaging to correlate the signal with the absolute concentration. The ternary plot in [Fig. 5f](#) shows that the concentration of the three compounds can be accurately measured with STE-SRS.

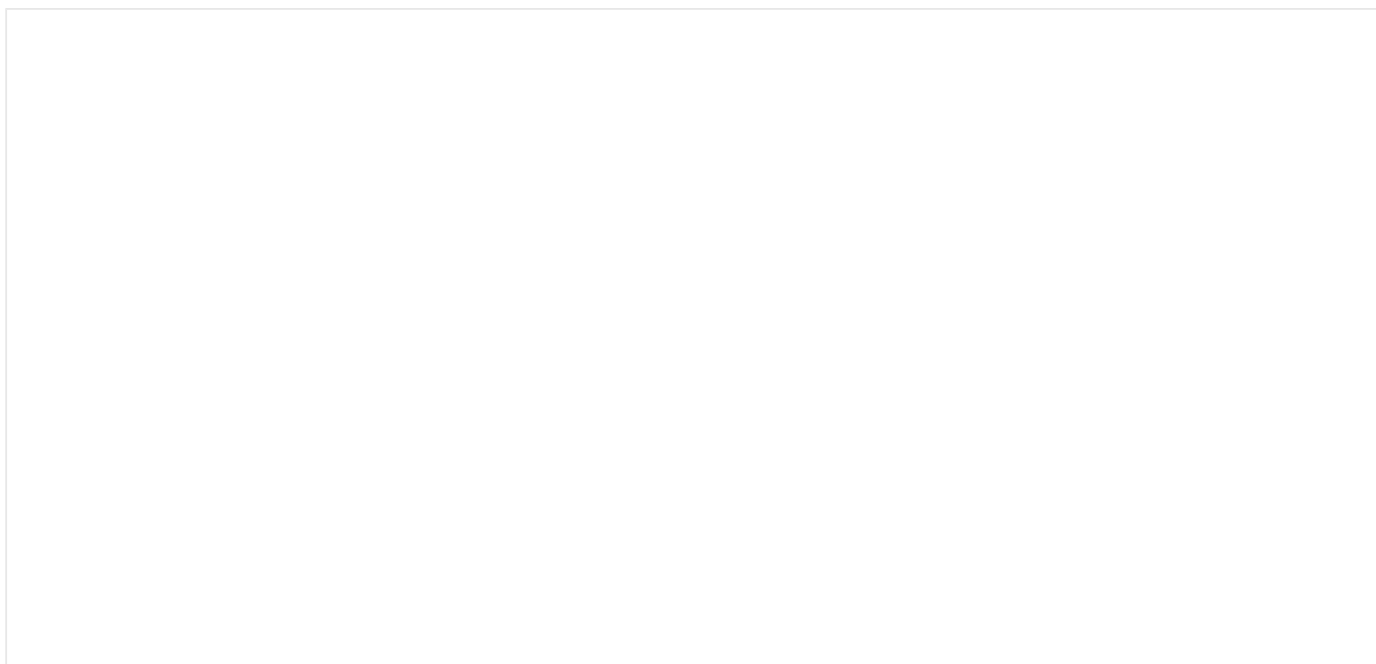
### **Imaging proteins and specific lipids *in vivo***

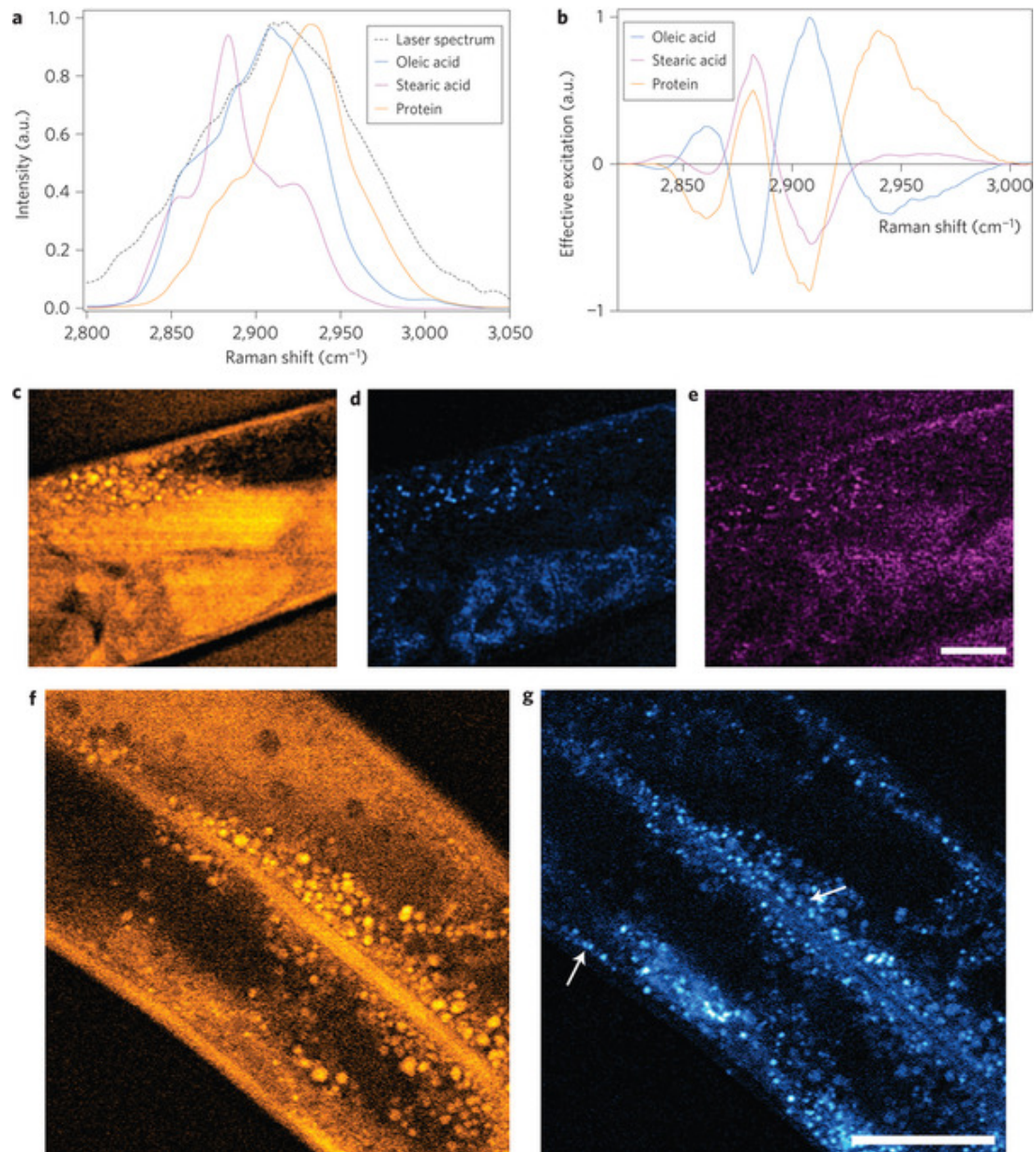
As an important application of STE-SRS, we demonstrated the selective imaging of different types of fatty acids *in vivo*. CARS microscopy has successfully been applied to study lipid storage in the nematode *Caenorhabditis elegans*, a common model organism in lipid research<sup>17</sup>, to overcome the shortcomings of lipid staining techniques that often fail

to stain all lipids uniformly<sup>18</sup>. We recently applied narrowband SRS imaging to image the distribution of unsaturated lipids in cells based on the characteristic CH vibration<sup>5</sup>. However, many lipid species do not have isolated vibrational bands. Thus, their distributions and dynamics cannot be probed by narrowband SRS.

We imaged the distributions of saturated and unsaturated fatty acids as well as proteins in *C. elegans*, which are the three main contributors to signal in the CH-region of Raman spectra of cells<sup>18, 19</sup>. Oleic and stearic acid were chosen as representative spectroscopic samples for unsaturated and saturated lipids, respectively, as they naturally occur in liquid and gel phases at room temperature. From the SRS spectra of the three pure compounds (Fig. 6a) we were able to generate three independent masks (Fig. 6b) that could selectively probe any of the three species in the presence of the other two. We could therefore selectively image a particular species by applying the corresponding mask to the SLM before image acquisition. Before imaging the actual worm sample, we first confirmed the correct choice of excitation masks in a test sample (Supplementary Fig. S3). We then took three images of the same region in the worm, one for each excitation mask, showing the distribution of protein (Fig. 6c), oleic acid (Fig. 6d) and stearic acid (Fig. 6e).

Figure 6: Imaging of lipid storage in *C. elegans*.





a, SRS spectra of oleic acid (cyan), stearic acid (magenta) and protein (orange) as computed from the spontaneous Raman library by normalizing with the measured laser excitation spectrum (dotted line). b, Spectral masks computed from spectra in a and used for the imaging. c–e, Spectral images taken from the same area of a *C. elegans*, applying spectral masks for protein (c), oleic acid (d) and stearic acid (e). Comparison of d and e shows that oleic and stearic acid deposits co-localize and that there are no isolated deposits of either species. Comparison of c and d shows that the lipid deposits further co-localize with protein-

dense organelles. f,g, Spectral images with protein and oleic acid masks, respectively, from a different region in the worm, further investigate this aspect. Arrows highlight both subdermal and intestinal lipid storage depots. Imaging speed: 30 s per frame, with 512 × 512 sampling. Scale bars, 25 μm.

• [Full size image \(1,020 KB\)](#)

• [Previous](#)

• [Figures index](#)

[figure](#)

A comparison of [Fig. 6d](#) and [e](#) shows that both compounds and their derivatives co-localize. In particular, there are no isolated storage areas that contain a single species only. Furthermore, fat deposits co-localize with areas of increased protein aggregation. [Figure 6f,g](#) and three-dimensional image stacks ([Supplementary Video 1](#)) from a different region in the worm show this in more detail. The arrows in the images indicate the two independent lipid storage areas, the subdermal and intestinal deposits. It is known that in intestinal cells, fat is stored in lysosome-related organelles<sup>17</sup>, which suggests why fat deposits are surrounded by the larger protein aggregates. With STE-SRS we can further see that the fat deposits of the subdermis are also surrounded by protein aggregates.

## Discussion

[Abstract](#)[Introduction](#)[Principle](#)[Results](#)[Discussion](#)[Methods](#)[References](#)[Acknowledgements](#)

[Author information](#)[Supplementary information](#)

Careful analysis of spectroscopic data to extract signal with a known spectral feature from complex and often noisy spectra is widely used, and is referred to as chemometrics<sup>20</sup>. In spontaneous Raman spectroscopy, chemometric methods have been used to understand hydrogen bonding<sup>21</sup>, detect glucose levels<sup>22</sup> and bone degeneration<sup>23</sup>, and image cells<sup>24</sup>. Although these methods have been used to analyse spectra computationally after data acquisition with a multi-element detector, multivariate optical computation has recently made use of a tailored multiband colour filter in front of a single-element detector<sup>25, 26</sup>. STE-SRS uses the same idea, but tailors the excitation spectra rather than the emission spectra.

With STE-SRS we have introduced a microscopy technique that combines fast speed with high chemical selectivity.

Several groups have recently advocated micro-spectroscopy based on spontaneous Raman scattering to complement rapid narrow band CARS imaging to provide spectroscopic analyses at selected positions<sup>19, 27</sup>. Our spectral SRS imaging provides spectroscopic information based on multiple Raman bands for every pixel of an image rather than for a few selected points.

In comparison with multiplex CARS microscopy<sup>12, 13, 14, 28</sup>, spectral SRS imaging has the advantage that no data processing is needed, because the SRS excitation spectra are identical to those of spontaneous Raman scattering<sup>5, 28</sup>. Furthermore, pixel dwell times in spectral SRS imaging can be orders of magnitude shorter than those in multiplex CARS<sup>14</sup>. In contrast to CARS pulse-shaping approaches<sup>29, 30, 31, 32, 33</sup>, STE-SRS requires amplitude-shaping instead of phase-shaping. Any phase manipulation, including that used in interferometric CARS<sup>34, 35</sup>, is prone to phase errors in biological samples, where refractive indices vary across the sample. In general, all CARS-related techniques are complicated by coherent image artefacts due to constructive and destructive spatial interferences at the dimension comparable to the diffraction limit spot<sup>36</sup>.

Note that if unknown chemical species exist in a sample, their Raman spectra need to be taken before STE-SRS microscopy can be carried out. STE-SRS does not diminish the need for Raman micro-spectroscopy. However, it significantly increases the speed at which chemical species can be mapped, which are often known *a priori* in biological samples. In principle, the number of species can be as high as the number of spectral pixels of tailored excitation. We also note that the principle of spectrally tailored excitation can be further extended to other modulation transfer techniques such as two-colour, two-photon absorption<sup>37</sup>, pump-probe<sup>38</sup> or stimulated emission<sup>39</sup>.

The combination of high specificity and high sensitivity of STE-SRS microscopy offers new potential for vibrational imaging in biology and medicine.

## Methods

[Abstract](#)[Introduction](#)[Principle](#)[Results](#)[Discussion](#)[Methods](#)[References](#)[Acknowledgements](#)[Author information](#)[Supplementary information](#)

The 1,064 nm narrowband Stokes beam was generated by a picosecond Nd:YVO<sub>4</sub> laser (HighQ, Picotrain), and the tunable broadband pump was obtained using a femtosecond Ti:sapphire laser (Coherent, Mira900) with a repetition rate of 76 MHz. The two lasers were synchronized using electronic synchronization (Coherent, Synchrolock) with timing jitter of <250 fs (refs [13,40](#)). To minimize nonlinear photodamage<sup>[41](#), [42](#), [43](#)</sup>, the pump beam was chirped to picoseconds by passing the beam through 35 cm of glass (Edmund Optics, NT63-091) without signal loss. Polarization pulse-shaping was achieved with a custom pulse-shaper from Biophotonic Solutions Inc. The pulse-shaper consisted of a grating (to disperse the broadband pulse) and a curved mirror (~1 m focal length to achieve a spectral resolution of 0.1 nm) to focus the spectral components onto a polarization SLM (CRI, SLM-640) in a 4*f* geometry in reflection mode<sup>[15](#)</sup>. The throughput of the pulse-shaper was ~55 ± 5% at a centre wavelength of 800 nm depending on the input polarization. The SLM was controlled using custom software control using LabView (National Instruments). To allow fast modulation between different polarization states (at 4 MHz), we used a combination of a custom-built Pockels cell (based on RTP crystals by Raicol) and polarization analyser. The Pockels cell was driven with a sine wave from the reference output of the lock-in amplifier (Stanford Research Systems, SR844RF), which was amplified to 1 W and efficiently coupled to the crystal with a resonant transformer. Pump and Stokes beams were spatially overlapped using an 850 nm long-pass mirror (Chroma Technology), temporally overlapped with the synchronization electronics by maximizing the cross-correlation signal on an autocorrelator (Spectra-Physics, 409 Autocorrelator) and coupled into a modified laser-scanning upright microscope (Olympus, BX61WI/FV300). We used a x60, 1.2 NA water immersion lens (Olympus, UPlanApo/IR) as excitation objective and the light was collected in transmission with a 1.4 NA oil condenser (Nikon). For imaging of biological samples, the average power was reduced to 15 mW for the pump and 120 mW for the Stokes. A large-area InGaAs photodiode (New England Photoconductors, I5-3-5) with a reverse bias of 12 V was used for detection of the narrowband Stokes beam, after blocking the spectrally modulated pump beam with a long-pass filter (Chroma Technology, HHQ925LP). The photodiode output was band-pass-filtered around the

modulation rate of 4 MHz with a custom-made bandpass filter. A high-frequency lock-in amplifier (Stanford Research Systems, SR844RF) was used to demodulate the Stokes intensity. A time constant of 10  $\mu$ s ('no filter' mode) was used for imaging and 1 s for the solution spectroscopy studies. The analog output of the lock-in amplifier was fed into an input of the microscope analog-to-digital converter to provide the intensity of a pixel.

## References

[Abstract](#)[Introduction](#)[Principle](#)[Results](#)[Discussion](#)[Methods](#)[References](#)[Acknowledgements](#)

[Author information](#)[Supplementary information](#)

1. Zumbusch, A., Holtom, G. R. & Xie, X. S. Three-dimensional vibrational imaging by coherent anti-Stokes Raman scattering. *Phys. Rev. Lett.* 82, 4142–4145 (1999).
  - [Show context](#)
2. Cheng, J. X. & Xie, X. S. Coherent anti-Stokes Raman scattering microscopy: instrumentation, theory, and applications. *J. Phys. Chem. B* 108, 827–840 (2004).
  - [Article](#)
  - [ISI](#)
  - [ADS](#)
  - [ChemPort](#)
3. Evans, C. L. & Xie, X. S. Coherent anti-Stokes Raman scattering microscopy: chemical imaging for biology and medicine. *Annu. Rev. Anal. Chem.* 1, 883–909 (2008).
  - [Article](#)
  - [ISI](#)
  - [ChemPort](#)
4. Ploetz, E., Laimgruber, S., Berner, S., Zinth, W. & Gilch, P. Femtosecond stimulated Raman microscopy. *Appl. Phys. B* 87, 389–393 (2007).
  - [Article](#)
  - [ISI](#)
  - [ChemPort](#)
5. Freudiger, C. W. *et al.* Label-free biomedical imaging with high sensitivity by stimulated Raman scattering microscopy. *Science* 322, 1857–1861 (2008).
  - [Article](#)
  - [ISI](#)
  - [ADS](#)
6. Ozeki, Y., Dake, F., Kajiyama, S., Fukui, K. & Itoh, K. Analysis and experimental assessment of the sensitivity of stimulated Raman scattering microscopy. *Opt. Express* 17, 3651–3658 (2009).
  - [Article](#)
  - [PubMed](#)
  - [ISI](#)
  - [ChemPort](#)
7. Nandakumar, P., Kovalev, A. & Volkmer, A. [Article](#) [PubMed](#) [ISI](#) [ADS](#) [ChemPort](#)

- Vibrational imaging based on stimulated Raman scattering microscopy. *New J. Phys.* 11, 033026 (2009).
- [Show context](#) 8. Evans, C. L. *et al.* Chemical imaging of tissue *in vivo* with video-rate coherent anti-Stokes Raman scattering microscopy. *Proc. Natl Acad. Sci. USA* 102, 16807–16812 (2005). [Article](#)
  - [Show context](#) 9. Saar, B. G. *et al.* Video-rate molecular imaging *in vivo* with stimulated Raman scattering. *Science* 330, 1368–1370 (2010). [Article](#) [PubMed](#) [ADS](#) [ChemPort](#)
  - [Show context](#) 10. Levenson, M. D. & Kano, S. S. *Introduction to Nonlinear Laser Spectroscopy* (Academic Press, 1988). [Article](#) [PubMed](#) [ISI](#) [ADS](#)
  - [Show context](#) 11. Kukura, P., McCamant, D. W. & Mathies, R. A. Femtosecond stimulated Raman spectroscopy. *Annu. Rev. Phys. Chem.* 58, 461–488 (2007).
  - [Show context](#) 12. Wurpel, G. W. H., Schins, J. M. & Muller, M. Chemical specificity in three-dimensional imaging with multiplex coherent anti-Stokes Raman scattering microscopy. *Opt. Lett.* 27, 1093–1095 (2002). [Article](#) [PubMed](#) [ISI](#) [ADS](#) [ChemPort](#)
  - [Show context](#) 13. Cheng, J. X., Volkmer, A., Book, L. D. & Xie, X. S. Multiplex coherent anti-Stokes Raman scattering microspectroscopy and study of lipid vesicles. *J. Phys. Chem. B* 106, 8493–8498 (2002). [Article](#) [PubMed](#) [ISI](#)
  - [Show context](#) 14. Rinia, H. A., Burger, K. N. J., Bonn, M. & Muller, M. Quantitative label-free imaging of lipid composition and packing of individual cellular lipid droplets using multiplex CARS microscopy. *Biophys. J.* 95, 4908–4914 (2008). [Article](#) [ChemPort](#)
  - [Show context](#) 15. Weiner, A. M. Femtosecond pulse shaping using spatial light modulators. *Rev. Sci. Instrum.* 71, 1929–1960 (2000). [Article](#) [PubMed](#) [ISI](#) [ADS](#)
  - [Show context](#) 16. Wise, B. M. *et al.* *PLS\_Toolbox 4.0 - Manual* (Eigenvector Research, [Article](#) [ISI](#) [ChemPort](#)

2006).

- [Show context](#) 17. Mullaney, B. C. & Ashrafi, K. C. *C. elegans* fat storage and metabolic regulation. *Biochim. Biophys. Acta* 1791, 474–478 (2009).
- [Show context](#) 18. Hellerer, T. *et al.* Monitoring of lipid storage in *Caenorhabditis elegans* using [PubMed](#) [ISI](#) coherent anti-Stokes Raman scattering (CARS) microscopy. *Proc. Natl Acad. Sci. USA* 104, 14658–14663 (2007).
- [Show context](#) 19. Slipchenko, M. N., Le, T. T., Chen, H. T. & Cheng, J. X. High-speed [Article](#) [PubMed](#) [ADS](#) vibrational imaging and spectral analysis of lipid bodies by compound Raman microscopy. *J. Phys. Chem. B* 113, 7681–7686 (2009).
- [Show context](#) 20. Mark, H. & Workman, J. *Chemometrics in Spectroscopy* (Academic [Article](#) [PubMed](#) [ISI](#) Press, 2007).
- [Show context](#) 21. Perera, P. N. *et al.* Observation of water dangling OH bonds around dissolved nonpolar groups. *Proc. Natl Acad. Sci. USA* 106, 12230–12234 (2009).
- [Show context](#) 22. Enejder, A. M. K. *et al.* Raman spectroscopy for noninvasive glucose [Article](#) [PubMed](#) [ADS](#) measurements. *J. Biomed. Opt.* 10, 031114 (2005).
- [Show context](#) 23. Schulmerich, M. V. *et al.* Noninvasive Raman tomographic imaging of canine [Article](#) [PubMed](#) bone tissue. *J. Biomed. Opt.* 13, 020506 (2008).
- [Show context](#) 24. Pully, V. V., Lenferink, A. & Otto, C. Raman-fluorescence hybrid [Article](#) [PubMed](#) microspectroscopy of cell nuclei. *Vib. Spectrosc.* 53, 12–18 (2010).
- [Show context](#) 25. Nelson, M. P., Aust, J. F., Dobrowolski, J. A., Verly, P. G. & Myrick, M. L. [Article](#) [ISI](#) Multivariate optical computation for predictive spectroscopy. *Anal. Chem.* 70, 73–82 (1998).
- [Show context](#) 26. Uzunbajakava, N., de Peinder, P., 't Hooft, G. W. & van Gogh, A. T. M. Low-cost [Article](#) [ISI](#)

spectroscopy with a variable multivariate optical element. *Anal. Chem.* 78, 7302–7308 (2006).

- [Show context](#) 27. Krafft, C. *et al.* A comparative Raman and CARS imaging study of colon tissue. *J. Biophoton.* 2, 303–312 (2009). [Article](#) ○ [PubMed](#) ○ [ISI](#)
- [Show context](#) 28. Rinia, H. A., Bonn, M. & Muller, M. Quantitative multiplex CARS spectroscopy in congested spectral regions. *J. Phys. Chem. B* 110, 4472–4479 (2006). [Article](#) ○ [ISI](#)
- [Show context](#) 29. Dudovich, N., Oron, D. & Silberberg, Y. Single-pulse coherently controlled nonlinear Raman spectroscopy and microscopy. *Nature* 418, 512–514 (2002). [Article](#) ○ [PubMed](#) ○ [ISI](#)
- [Show context](#) 30. van Rhijn, A. C. W., Postma, S., Korterik, J. P., Herek, J. L. & Offerhaus, H. L. Chemically selective imaging by spectral phase shaping for broadband CARS around 3000 cm<sup>-1</sup>. *J. Opt. Soc. Am. B* 26, 559–563 (2009). [Article](#) ○ [PubMed](#) ○ [ISI](#) ○ [ADS](#) ○ [ChemPort](#)
- [Show context](#) 31. Marks, D. L., Geddes, J. B. & Boppart, S. A. Molecular identification by generating coherence between molecular normal modes using stimulated Raman scattering. *Opt. Lett.* 34, 1756–1758 (2009). [Article](#) ○ [ISI](#) ○ [ADS](#)
- [Show context](#) 32. Oron, D., Dudovich, N. & Silberberg, Y. All-optical processing in coherent nonlinear spectroscopy. *Phys. Rev. A* 70, 23415 (2004). [Article](#) ○ [PubMed](#) ○ [ISI](#) ○ [ADS](#)
- [Show context](#) 33. Roy, S., Wrzesinski, P., Pestov, D., Dantus, M. & Gord, J. R. Single-beam coherent anti-Stokes Raman scattering (CARS) spectroscopy of gas-phase CO<sub>2</sub> via phase and polarization shaping of a broadband continuum. *J. Raman Spectrosc.* 41, 1194–1199 (2010). [Article](#) ○ [ADS](#)
- [Show context](#) 34. Evans, C. L., Potma, E. O. & Xie, X. S. N. Coherent anti-Stokes Raman scattering spectral interferometry: determination of the real and imaginary components of nonlinear susceptibility  $\chi^{(3)}$  for vibrational microscopy. *Opt. Lett.* 29, 2923–2925 (2004). [Article](#) ○ [ISI](#) ○ [ADS](#)
- [Show context](#) 35. Jurna, M., Korterik, J. P., Otto, C., Herek, J. L. & Offerhaus, H. L. Background free CARS imaging by phase sensitive heterodyne CARS. *Opt. Express* 16, 15863–  
<http://www.nature.com/nphoton/journal/vaop/ncurrent/full/nphoton.2010.294.html> (26 of 30) [1/28/2011 10:44:35 AM] [Article](#) ○ [PubMed](#) ○ [ISI](#)

Backround free CARS imaaina by phase sensitive heterodyne CARS. *Opt. Express* 16, 15863–

15869 (2008).

- [Show context](#) 36. Cheng, J. X. & Xie, X. S. Green's function formulation for third-harmonic generation microscopy. *J. Opt. Soc. Am. B* 19, 1604–1610 (2002).  
◦ [Article](#) ◦ [PubMed](#) ◦ [ISI](#) ◦ [ADS](#)
  
- [Show context](#) 37. Fu, D., Ye, T., Matthews, T. E., Yurtsever, G. & Warren, W. S. Two-color, two-photon, and excited-state absorption microscopy. *J. Biomed. Opt.* 12, 054004 (2007).  
◦ [Article](#) ◦ [ISI](#) ◦ [ADS](#) ◦ [ChemPort](#)
  
- [Show context](#) 38. Fu, D. *et al.* Probing skin pigmentation changes with transient absorption imaging of eumelanin and pheomelanin. *J. Biomed. Opt.* 13, 054036 (2008).  
◦ [Article](#) ◦ [PubMed](#) ◦ [ChemPort](#)
  
- [Show context](#) 39. Min, W. *et al.* Imaging chromophores with undetectable fluorescence by stimulated emission microscopy. *Nature* 461, 1105–1109 (2009).  
◦ [Article](#) ◦ [PubMed](#)
  
- [Show context](#) 40. Jones, D. J. *et al.* Synchronization of two passively mode-locked, picosecond lasers within 20 fs for coherent anti-Stokes Raman scattering microscopy. *Rev. Sci. Instrum.* 73, 2843–2848 (2002).  
[Article](#) ◦ [PubMed](#) ◦ [ISI](#) ◦ [ADS](#) ◦ [ChemPort](#)
  
- [Show context](#) 41. Hopt, A. & Neher, E. Highly nonlinear photodamage in two-photon fluorescence microscopy. *Biophys. J.* 80, 2029–2036 (2001).  
◦ [Article](#) ◦ [ISI](#)
  
- [Show context](#) 42. Nan, X. L., Potma, E. O. & Xie, X. S. Nonperturbative chemical imaging of organelle transport in living cells with coherent anti-stokes Raman scattering microscopy. *Biophys. J.* 91, 728–735 (2006).  
◦ [Article](#) ◦ [PubMed](#) ◦ [ISI](#) ◦ [ChemPort](#)
  
- [Show context](#) 43. Fu, Y., Wang, H. F., Shi, R. Y. & Cheng, J. X. Characterization of photodamage in coherent anti-Stokes Raman scattering microscopy. *Opt. Express* 14, 3942–3951 (2006).  
◦ [Article](#) ◦ [PubMed](#) ◦ [ISI](#) ◦ [ADS](#)
  
- [Show context](#) [Article](#) ◦ [PubMed](#) ◦ [ISI](#) ◦ [ADS](#)

[Download references](#)

## Acknowledgements

---

[Abstract](#)[Introduction](#)[Principle](#)[Results](#)[Discussion](#)[Methods](#)[References](#)[Acknowledgements](#)

[Author information](#)[Supplementary information](#)

The authors thank Linjiao Luo and Aravinthan Samuel for providing the *C. elegans* sample for initial testing, B. Saar and Sijia Lu for helpful discussions and comments on the manuscript, and Xu Zhang for assisting in the final concentration measurements. C.W.F. acknowledges Boehringer Ingelheim Fonds for a PhD Fellowship. This work was supported by the National Institutes of Health (NIH) Director's Pioneer Award and NIH TR01 grant 1R01EB010244-01.

## Author information

---

[Abstract](#)[Introduction](#)[Principle](#)[Results](#)[Discussion](#)[Methods](#)[References](#)[Acknowledgements](#)

[Author information](#)[Supplementary information](#)

## Affiliations

### 1. Department of Physics, Harvard University, Cambridge, Massachusetts 02138, USA

Christian W. Freudiger

### 2. Department of Chemistry and Chemical Biology, Harvard University, Cambridge, Massachusetts 02138, USA

Christian W. Freudiger, Wei Min, Gary R. Holtom & X. Sunney Xie

### 3. Biophotonic Solutions Inc., East Lansing, Michigan 48823, USA

Bingwei Xu

### 4. Department of Chemistry and Department of Physics, Michigan State University, East Lansing,

Michigan 48824, USA

Marcos Dantus

## Contributions

C.W.F., W.M. and X.S.X. conceived the idea and drafted the manuscript. C.W.F. and G.R.H. built the instrument, B.X. and

M.D. designed and built the pulse-shaper, and C.W.F. conducted the experiments.

## Competing financial interests

## Corresponding author

Correspondence to: [X. Sunney Xie](#)

## Supplementary information

[Abstract](#)[Introduction](#)[Principle](#)[Results](#)[Discussion](#)[Methods](#)[References](#)[Acknowledgements](#)

[Author information](#)[Supplementary information](#)

### Movies

1. [Supplementary information \(31.6 MB\)](#)

### PDF files

1. [Supplementary information \(996 KB\)](#)

• *Nature Photonics*

• ISSN 1749-4885

• EISSN 1749-4893

- [About NPG](#)
- [Privacy policy](#)
- [Nature News](#)
- [Contact NPG](#)
- [Legal notice](#)
- [Naturejobs](#)
- [RSS web feeds](#)
- [Accessibility statement](#)
- [Nature Asia](#)
- [Help](#)
- [Terms](#)
- [Nature Education](#)

Search:

Go

© 2010 Nature Publishing Group, a division of Macmillan Publishers Limited. All Rights Reserved.

partner of AGORA, HINARI, OARE, INASP, CrossRef and COUNTER